Volume 16 | Number 21 | 7 June 2014 | Pages 9669–10234

PCCP

Physical Chemistry Chemical Physics
www.rsc.org/pccp

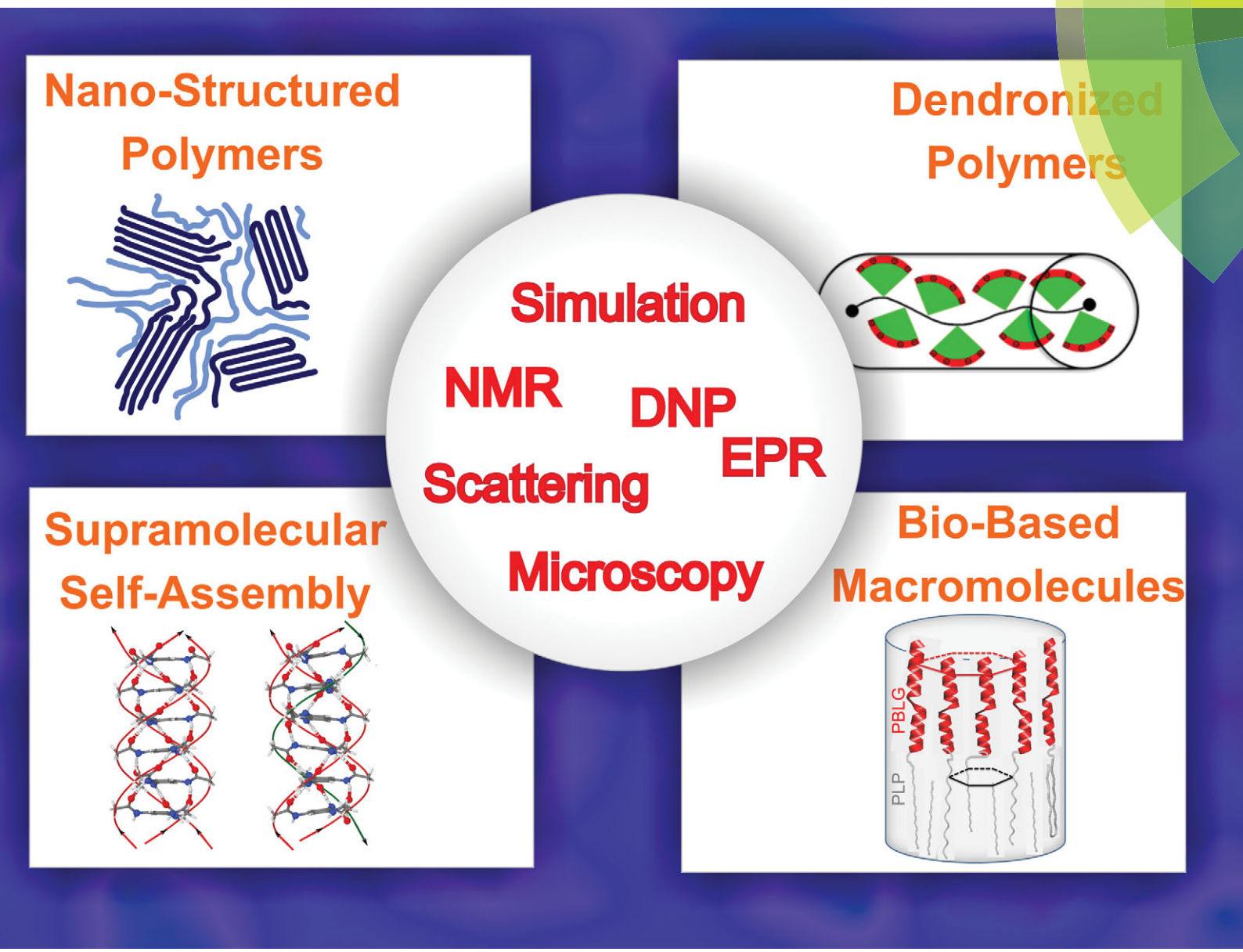

ISSN 1463-9076

ROYAL SOCIETY OF CHEMISTRY

PERSPECTIVE
H. W. Spiess *et al.*
Advanced magnetic resonance strategies for the elucidation of nanostructured soft matter

PCCP

PERSPECTIVE

View Article Online
View Journal | View Issue

Open Access Article. Published on 18 2013. Downloaded on 14.03.2025 11:04:40.
This article is licensed under a Creative Commons Attribution 3.0 Unported Licence.

Cite this: *Phys. Chem. Chem. Phys.*, 2014, **16**, 9700

Advanced magnetic resonance strategies for the elucidation of nanostructured soft matter

R. Graf,[a] M. R. Hansen,[ab] D. Hinderberger,[ac] K. Muennemann[a] and H. W. Spiess*[a]

Received 31st October 2013,
Accepted 16th December 2013

DOI: 10.1039/c3cp54614d

www.rsc.org/pccp

An overview is given on advanced magnetic resonance strategies and techniques, both nuclear magnetic resonance (NMR) and electron paramagnetic resonance (EPR), as applied to nanostructured soft matter. In addition, the combination of the two forms of spectroscopy to enhance signal intensity in NMR by means of dynamic nuclear polarization (DNP) is described. It is shown how these techniques can provide unique information on the structure of soft matter as well as the local dynamics of the constituents. Examples of recent applications are described, including dendronized and thermoresponsive polymers, hydrogels, synthetic and bio-inspired polymers, as well as polypeptides and biopolymers.

1 Introduction

The function of complex synthetic as well as natural systems is often achieved by separating regions of order and disorder.[1] Examples are semi-crystalline synthetic polymers or polymer systems composed of different repeat units, *i.e.* polymer blends or copolymers. Likewise biomacromolecules, such as proteins, are often composed of well-ordered regions with α-helices or β-sheets, interlinked by conformationally disordered chain segments.[2] Moreover, incompatibility of building blocks, *e.g.*, backbone and side groups in macromolecules, or non-covalent interactions, such as hydrogen bonds, ionic forces or π–π-interactions lead to self-organization.[3] In all these structures the different units are spatially separated and, therefore, can display vastly different dynamics.

Even if highly ordered on a local scale, such systems often do not crystallize. Therefore, their atomic resolution structures cannot be determined by conventional X-ray or neutron scattering techniques.[4] In order to provide insight into the organization of such materials to further understand their function, advanced methods of characterization are needed to probe both structure and dynamics simultaneously.[5]

If structural information on a molecular level is sought, *site-selectivity* is required. Moreover, for macroscopic organization, mechanical properties, and transport of ions or charges in highly viscous materials or even solids, 'slow' dynamics on time scales longer than nano- or microseconds are particularly relevant. While several techniques meet one or the other requirement for elucidating structure and dynamics, nuclear magnetic resonance (NMR) spectroscopy[6,7] meets all needs and rapid development of NMR methods is still ongoing.[8] Likewise, electron paramagnetic resonance (EPR) spectroscopy of spin labels and spin probes in synthetic and biomacromolecules is enjoying a remarkable revival, due to improved microwave technology.[9,10] These advances now allow routine applications of pulsed EPR methods and high-field EPR with similar improvements as in high-field NMR. However, no single technique can provide the required information. Instead, a combination of complementary methods is required as sketched in Fig. 1. This also includes the combination of experimental techniques and computer simulations. Remarkably, recent developments in magnetic resonance have been recognized

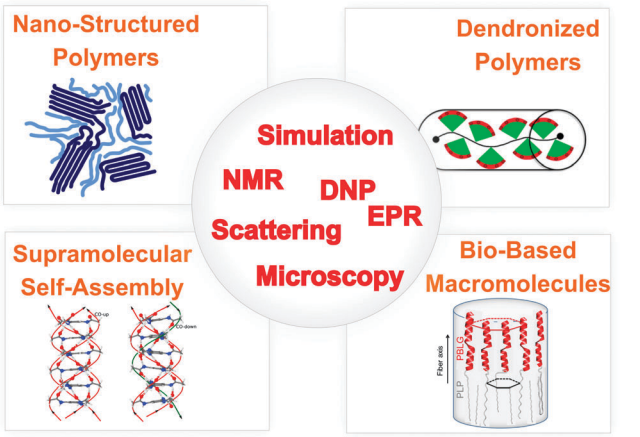

Fig. 1 Overview of systems, phenomena and techniques for elucidating the interplay between structure and dynamics in nanostructured soft matter.

[a] *Max Planck Institute for Polymer Research, Ackermannweg 10, 55128 Mainz, Germany. E-mail: spiess@mpip-mainz.mnpg.de*
[b] *Interdisciplinary Nanoscience Center (iNANO) and Department of Chemistry, Aarhus University, Gustav Wieds Vej 14, DK-8000 Aarhus C, Denmark*
[c] *Martin-Luther-Universität Halle-Wittenberg, Institute of Chemistry, Von-Danckelmann-Platz 4, 06120 Halle (Saale), Germany*

This journal is © the Owner Societies 2014

Open Access Article. Published on 18 2013. Downloaded on 14.03.2025 11:04:40.
This article is licensed under a Creative Commons Attribution 3.0 Unported Licence.

by a large number of papers in Physical Chemistry Chemical Physics, *e.g.*, see ref. 11–14.

Despite the wealth of information NMR spectroscopy provides, it suffers from its inherently low signal intensity due to the low magnetic moment of nuclei. In contrast, the magnetic moment of electrons is almost three orders of magnitude higher. This can be exploited, *i.e.*, by combining NMR and EPR, transferring magnetization from electrons to nuclei. This possibility was realized early on and was called dynamic nuclear polarization (DNP).[15,16] Similar to EPR itself, DNP has experienced a remarkable revival in recent years and is now applied to biopolymers in both solution and the solid state.[17]

In this Perspective Article we briefly introduce magnetic resonance in general, followed by a more detailed description of specific examples, which demonstrate the application of such techniques to study bio-inspired synthetic macromolecules and biopolymers, mostly taken from our own recent work.

1.1 Solid state NMR and pulsed EPR techniques for analyzing structure and dynamics

NMR spectroscopy today is an indispensable tool in chemistry, physics and life sciences. The introduction of Fourier transform NMR and its extension to two- and higher dimensions made it possible to perform in addition to ^{1}H NMR, highly informative spectroscopy of rare nuclei, such as ^{13}C or ^{15}N despite their formidably low sensitivity.[6] These techniques are now mainly applied to study biomacromolecules in solution,[18] but increasingly also in the solid state.[19] In the latter case multidimensional NMR techniques were actually developed for synthetic polymers first.[7] Advances in solid state NMR under fast Magic Angle Spinning (MAS) offered an attractive way to elucidate the packing and local dynamics of the building blocks in supramolecular assemblies; for a review of the early examples, see ref. 20.

In the early days of magnetic resonance, NMR and EPR spectroscopy were developed in parallel and often by the same people.[21,22] Later on the two techniques largely separated, but as mentioned above, recent developments in microwave technology have allowed spectroscopists to use pulse methods in EPR as well and it is rewarding to see the two 'sister spectroscopies' merge again. In fact, the current revival of EPR (ESR) spectroscopy in macromolecular science is largely due to the development of pulsed methods in groups active in both solid state NMR and EPR.[23,24] Together with site directed spin labeling,[25] the structure of biomacromolecules and supramolecular assemblies can now be probed on the nanometer scale,[26] which nicely augments the sub-nm information provided by NMR. A singular advantage of MR methods is the fact that structure determination does not require single crystals needed for X-ray, or neutron scattering. Therefore, MR can be applied to condensed matter in all forms, including liquids, crystalline solids, disordered solids, liquid crystals and even gases.[27]

Signals originating from hydrogen-bonded protons are well separated in ^{1}H MAS NMR spectra, typically resonating between 8 and 20 ppm.[28] Hence, the ^{1}H chemical shift provides semiquantitative information about the strength of hydrogen bonds.[29] In addition, the ^{1}H chemical shift is also a sensitive probe of so-called ring currents associated with aromatic moieties. These are observed as a low field shift compared to the corresponding liquid state NMR signal and may thereby serve as a direct indicator of π–π interactions. Likewise, the low field shift can be simply related to the crystal packing *via* so-called Nucleus Independent Chemical Shift (NICS) maps.[30] This augments the well-known sensitivity of ^{13}C NMR chemical shifts to local conformation, manifested, *e.g.*, by the *γ-gauche* effect.[31] Detailed packing information is obtained from distance measurements between specific proton sites at adjacent building blocks *via* high resolution double quantum (DQ) solid state NMR under MAS.[20,32,33] This is particularly important for supramolecular assemblies involving aromatic groups and functional polymers for organic electronics.[34]

Solid state NMR, however, is probably even more powerful for probing the time scale and amplitude of rotational motions.[7,35] For instance, disk shaped aromatics often stack into columnar structures as part of discotic liquid crystals (DLC),[36] which are of great interest because of their function in organic electronics.[37,38] In the liquid crystalline phase the disks rotate around the column axis.[35] A particularly simple way of characterizing such restricted molecular dynamics is provided by the dynamic order parameter, $0 \leq S \leq 1$. It is defined as the ratio between the motionally averaged and the static anisotropic NMR interaction, *e.g.*, dipole–dipole coupling, anisotropic chemical shift, or quadrupole coupling. For the rotation of disks in a perfectly packed column, $S = 0.5$ for ^{13}C–^{1}H dipole–dipole coupling, or ^{2}H quadrupole coupling, probing the C–H (C–D) bond direction.[35] Imperfections of the packing in the liquid crystalline phase, where disks can be tilted towards the column axis, lead to reduction of S below 0.5 and values as low as 0.15 have been found.[39] Thus, S provides both dynamic and structural information. In general, solid state NMR yields site selective information about the amplitudes and time scales of molecular motions over broad ranges of length and time; for a recent review see ref. 35.

The information about structure and dynamics of soft matter that EPR can provide is very similar.[9,10] For synthetic polymers, biopolymers, and supramolecular assemblies, nitroxide spin probes and spin labels are particularly useful.[40] In solution, their EPR spectra are governed by the *g*-factor and the hyperfine splitting (denoted as a) due to the ^{14}N nucleus of the NO group. In solution, the former determines the frequency of the center of the triplet arising from the hyperfine coupling. Both parameters are sensitive to the electronic environment. In the solid state, the anisotropy of the *g*-tensor leads to broad characteristic EPR line shapes, similar to those in solid state NMR. EPR spectra are averaged by rotational motions, yet on the ns timescale rather than the μs scale that is relevant in NMR.[7,9] This motional averaging has been exploited extensively in macromolecular science, due to the pioneering work of J. Freed.[41] Moreover, similar to NMR, the dipole–dipole couplings between electron and nuclear spins can be exploited to determine intermolecular distances below one nm. The much stronger couplings between

Open Access Article. Published on 18 2013. Downloaded on 14.03.2025 11:04:40.
This article is licensed under a Creative Commons Attribution 3.0 Unported Licence.

two electron spins can be used to probe distances up to about 8–10 nm. These types of measurements are achieved by pulsed electron-nuclear (ENDOR) or double electron-electron resonance (DEER) techniques, respectively.[23,24]

2 EPR studies of dendronized polymers in solution and in the solid state

2.1 Identifying molecular objects by EPR spectroscopy

Synthetic nanostructured systems are intricately connected with high precision through chemical synthesis. Dendrimers can be viewed as early examples of complex yet highly precise supramolecular structures.[42] Dendronized polymers (denpols), highly precise polymers with dendronized side chains on every repeat unit, are an exciting new class of materials.[43] Denpols combine the possibility to create large, polymeric structures with the precision and versatility of dendrimers, which distinguishes them from, *e.g.* hyperbranched polymers.[44] Recently, continuous wave (CW) EPR has been shown to be an extremely versatile tool to study the nanoscale of thermoresponsive denpols and polymers in general.[45,46] Distinct from responsive polymers, dendronized polymers can be considered as *molecular objects*, *i.e.*, nanostructured objects exhibiting a persistent shape, independent of their immediate environment, and having a well-defined envelope.[43]

To qualify as a molecular object, the solution structure of a chemical entity should not differ significantly from that in the solid state. For most macromolecules marked differences between liquid and solid state structures are observed, even for biomacromolecules. For instance, by double electron electron resonance (DEER) spectroscopy we have recently shown that even for the well-folded protein human serum albumin (HSA), the solution structure differs significantly from the crystal structure.[47–49] The entry points of fatty acids into HSA are distributed highly symmetrically over the surface of the protein in solution to optimize fatty acid uptake, while an asymmetric distribution is observed in the crystal structure. Remarkably, the solution structure of the highly related bovine serum albumin was in good agreement with the crystal structure.[48,49]

Among other advantages, denpols have tunable thicknesses and high persistence lengths.[43] From the structural point of view, they are linear polymers whose repeat units all carry dendrons of variable generation (the number of branching units, n; here, the number of terminal groups is $2n$) and termination (the end groups of the outer shell). We have studied denpols that are based on poly(methacrylate) and carry positively charged ammonium groups at their peripheral end groups, see Fig. 2.[50–52] The densely packed dendrons around the backbone render the polymer's shape cylindrical and provide it with variable stiffness and diameter. Recently, a generation 5 species has been reported that can be considered as a molecular object due to its considerable stiffness (persistence length $l_p \approx 30$ nm) and the fact that it largely maintains its cross-section geometry when deposited on a solid substrate.

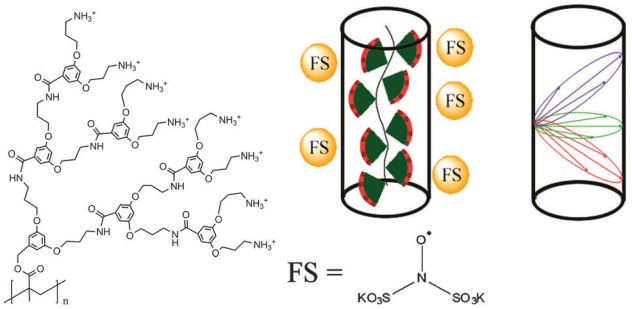

Fig. 2 The molecular structure of de-PG3 with the peripheral ammonium groups is shown on the left. In the center, the coordination of FS on the cylindrical surface of the dendronized polymers is shown schematically. The possible distances of a spin on the surface of a cylinder to points on the surface are sketched in the figure on the right. The red, blue and green ellipses represent only three of an infinite number of possible orientations. Reprinted with permission of the American Chemical Society.

To study the shape and size of dendronized polymers in solution, we have used DEER spectroscopy, measuring the dipolar coupling between two or more electron spins, which depends on the interspin distance, r.[52] In practice, distance distributions ranging from approximately 1.5 to 8 nm can be obtained. In this way, we determined the size (thickness) of different generations of cylindrical denpols in solution. The claim that any conventional polymer is rendered into a molecular object by attaching high generation dendrons to each of its main chain repeat units was then substantiated by showing that the difference between the solid state radius and the solution size decreases with each successive generation. Furthermore, the DEER-based characterization of dianionic spin probes that self-assemble close to the surface of cationic denpols is an indirect yet precise method to determine the effective spatial constitution and diameter of large, charged objects in solution.

Modern EPR spectroscopy, in particular for structural elucidation of proteins, heavily relies on covalent attachment by site-directed spin labeling (SDSL).[53] Instead of chemically labeling the denpols, here one can elegantly rely on the self-assembly of the doubly negatively charged spin probe Fremy's salt (FS, potassium nitrosodisulfonate, also shown in Fig. 2) at the denpol ammonium surface layer of high positive charge density. The electrostatic attachment of FS spin probes to the denpols of varying generation (de-PG1 to de-PG4) was verified by CW EPR, as observed before for polyelectrolytes.[54] This allows us to use this approach for nanoscale distance measurements by DEER.

2.2 Data analysis and comparison with other methods

Previous AFM studies indicate that in the solid state the diameter of the denpols PG1-4 grows with increasing generation; PG-1 is approx. 0.8 nm thick and PG-4 about 4 nm. Since one can assess distances between approx. 1.5 and 8 nm with DEER, one may determine the solution diameter of the denpols,

This journal is © the Owner Societies 2014

Open Access Article. Published on 18 2013. Downloaded on 14.03.2025 11:04:40.
This article is licensed under a Creative Commons Attribution 3.0 Unported Licence.

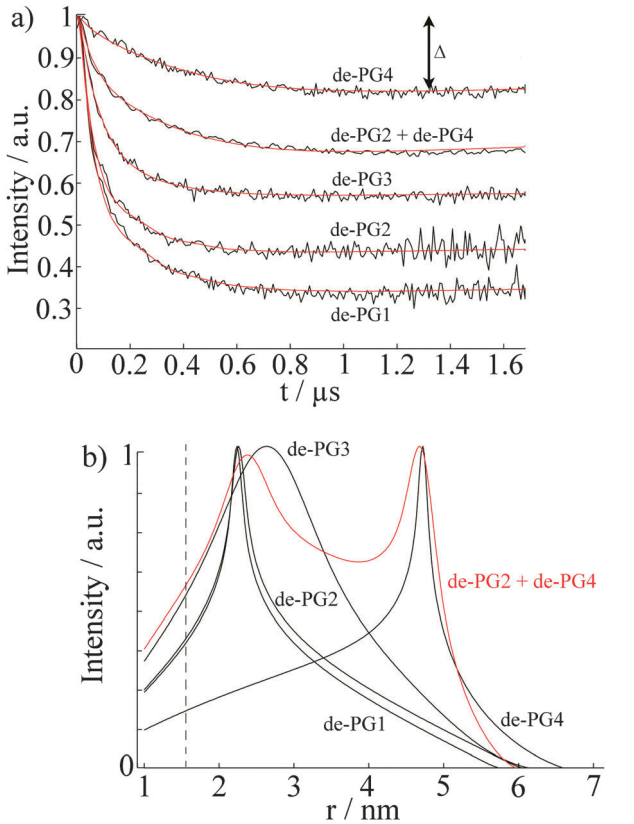

Fig. 3 (a) The normalized time-traces, *i.e.* form factors, of the dipolar evolution for FS and denpols of different generations. The red lines indicate the fits of the experimental time-traces (black lines) calculated from the assumed cylindrical distribution of Fremy's salt around the denpols. (b) Distance distributions of spins in denpol solutions containing Fremy's salt. The distributions were calculated from the fits of the experimental time-traces, presented in (a). The red line represents the bimodal distribution determined for a mixture of de-PG2 and de-PG4. The dotted line indicates the minimal observable distance, r_{min}. Reprinted with permission of the American Chemical Society.

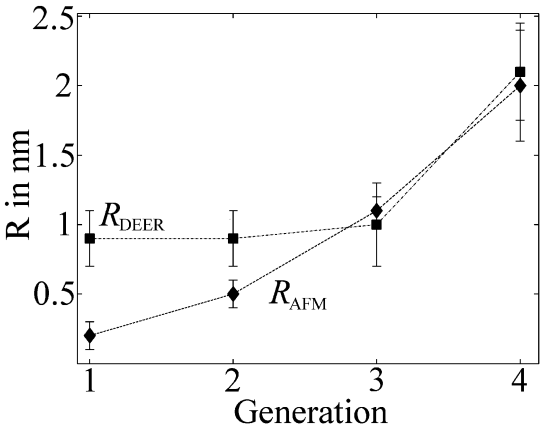

Fig. 4 Radii of the different generations of dendronized polymers determined from solution and solid state measurements plotted *versus* denpol generation. Values marked R_{DEER} stem from analysis of the data presented in Fig. 3 and are representative for the size of the molecules in solution (filled squares). Values marked RAFM stem from AFM tapping of the protected denpols PG1-4 heights published before and are representative for the size in the solid state (filled diamonds). Reprinted with permission of the American Chemical Society.

which might be difficult or would require substantial effort (*e.g.*, SANS) to access by other means. Fig. 3a depicts the time traces of the dipolar evolution for FS ions in the presence of denpols of different generations. We also show fits (red traces) based on a physical model assuming a uniform distribution of the probes on the surface of a cylinder, described in detail elsewhere.[50]

Given the highly constrained molecular shapes of dendronized polymers, we assumed that the spin probes are distributed independently and uniformly on the lateral surface of circular cylinders. For this geometry an analytic expression for the distance distribution $P(r)$ was derived.[50] Fits of DEER time traces to this analytical expression are shown in Fig. 3a. They yield the distance distribution of FS on the cylindrical surface shown in Fig. 3b. The most probable inter-probe distance R_{DEER}, after correction for the finite size of the probe and its thermal motion, corresponds to the diameter of the effective cylinder and, hence, the approximate thickness of the nanoscopic objects. The denpol radii obtained *via* DEER are graphically depicted in Fig. 4 together with the radii determined on the basis of the AFM tapping heights (R_{AFM}) for the denpols with protected terminal amines on mica.[43] The latter can be considered to correspond to the radii of the neutral denpol-analogues in the solid state, since the samples are dried on a mica surface during the preparation process. When comparing the results deduced from AFM and DEER, the following aspects have to be taken into account: (i) AFM is known to underestimate heights of objects on surfaces; (ii) DEER measurements have a lower limit of $\sim$1.5 nm and are based on the electrostatic self-assembly of FS, for which the surface distribution through thermal motion has to be corrected.[50] The corrected radii so obtained are shown in Fig. 4, while the distribution functions in Fig. 3 are plotted as a function of the unscaled radii.

This approach of fitting DEER time domain data to analytical solutions of cylindrical spin probe distributions was also checked by performing DEER experiments on mixtures of de-PG2 and de-PG4. The data were fitted with a bimodal distribution based on two cylinders. The time-trace is also shown in Fig. 3a, while the respective distance distribution is shown in red in Fig. 3b. Analysis of the mixed sample supports the picture of two individual, significantly different generations of denpols which can be described by the cylindrical shell model.

In summary, these studies show that DEER is a fast and precise method to determine the size of nanoscopic objects in solution. In the case presented here, a simple geometrical model was sufficient to determine the thickness of a cylindrical nano-sized object in solution and supports the idea that dendronized polymers (even of generation as low as 3) can be considered as molecular objects with an environment-independent, persistent shape. In particular, it was found that the size of the ammonium-terminated denpols in solution becomes similar to the size in the solid state as the generation grows. In the particular case of ammonium-terminated denpols addressed here, Fremy's salt could be applied as a negatively

Open Access Article. Published on 18 2013. Downloaded on 14.03.2025 11:04:40.
This article is licensed under a Creative Commons Attribution 3.0 Unported Licence.

charged spin probe, although a correction accounting for the thermal motion of the probe in the electrostatic potential is necessary. This provides a simple alternative to the more difficult method of spin labeling the periphery of a molecular object.

In follow-up studies it could furthermore be shown how amphiphilic molecules (*e.g.*, fatty acids) are taken up into these charged denpols, and by combining two spin probes (FS on the surface and spin-labeled fatty acids inside the denpols), it could even be shown how many molecules are taken up into denpols and how these are oriented within the large polymeric scaffold.[51] Also, in a combined TEM/EPR study the use of charged denpols as carriers for small molecules and the formation of structures in the ten to hundred nm scale could be elucidated.[52]

Finally, the strategy to determine shapes and sizes of macromolecules with EPR methods may be expanded to other complex self-assembled supramolecular systems, since *e.g.* attraction of spin-probes to large macromolecules due to hydrophobicity/hydrophilicity is well documented.

3 NMR studies of structure and dynamics in synthetic and bio-based polymers

One of the key challenges for the future sustainable use of polymers is to make the production of these independent of oil resources. This has inspired researchers to employ plant oils and other biomass-derived chemicals as feedstock for the production of bio-based polymers.[55–58] Another important strategy is to take advantage of enzymatic reactions that facilitate a green chemistry route to such polymeric materials.[59] However, a concern remains whether the chemical and physical properties of bio-based polymers match those synthesized from petrochemical sources.

From a structural point-of-view this encompasses the influence of the bio-based groups on (i) how the polymer material crystallizes to form nano-structured domains,[61] utilizing non-covalent interactions such as hydrogen-bonding and π–π-stacking,[62–64] (ii) crystallinity and chain conformations,[65] and (iii) whether the bio-based groups themselves are conformationally stable when built into a polymeric structure. Such structural properties can influence the melting point and lead to potentially stiffer or more flexible materials.

3.1 Influence of ester groups on the physical properties of polyolefins

In a recent study focusing on the incorporation of ester groups in polyethylene, forming aliphatic long-chain polyesters (ALCPEs) *via* ring-opening metathesis polymerization (ROMP) of cyclic olefins,[66–68] we have characterized the crystalline and amorphous domains of a polymer with the aim of quantifying the partitioning of the ester groups.[60] Fig. 5a displays the melting temperatures of a series of ALCPEs plotted as a function of the methylene-to-ester ratio (M/E). This plot clearly shows that an increase of the number of methylene units

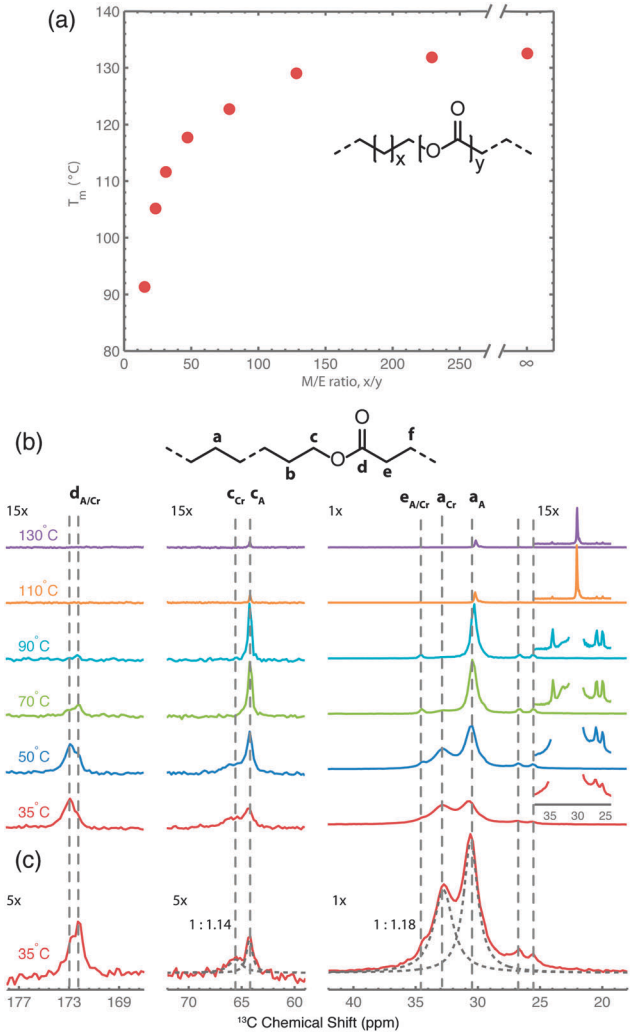

Fig. 5 (a) Plot of the melting temperature for ALCPEs as a function of the methylene-to-ester ratio (M/E) synthesized *via* ROMP using a first-generation Grubbs catalyst. (b) Variable-temperature $^{13}C\{^1H\}$ CP/MAS NMR spectra of an ALCPE with a M/E ratio of 31 (ME31) recorded from 35 to 130 °C. (c) Quantitative ^{13}C MAS NMR spectrum of ME31 illustrating the deconvolution into crystalline (Cr) and amorphous (A) fractions (dashed lines) for the methylene and α-methoxy carbon groups. Reprinted with permission from ref. 60. Copyright 2013, American Chemical Society.

between the ester groups causes a gradual increase in the melting temperature, converging toward the melting temperature of HDPE. Such a behavior is similar to that found on incorporating aliphatic side groups in polyethylene at well-defined positions.[69,70] To investigate the partitioning of the ester groups over the crystal and amorphous phases, we have employed a combination of variable-temperature (VT) solid state $^{13}C\{^1H\}$ CP/MAS NMR and quantitative ^{13}C MAS NMR as summarized in Fig. 5b, and solid state $^{13}C\{^1H\}$ INEPT NMR together with liquid-state ^{13}C NMR (see Fig. S7 and S8 in ref. 60). This allows us to differentiate between rigid and flexible parts of the polymer material.[7] The two main ^{13}C resonances at 30.8 and 32.8 ppm are assigned to the non-crystalline and the crystalline all-*trans* methylene conformations, respectively.[71] The α-methoxy carbons also display two signals: one at 64.3 ppm, identified *via*

Open Access Article. Published on 18 2013. Downloaded on 14.03.2025 11:04:40.
This article is licensed under a Creative Commons Attribution 3.0 Unported Licence.

$^{13}C\{^{1}H\}$ INEPT NMR as arising from the more flexible fraction in *gauche* conformation, and a second peak at 65.7 ppm from the crystalline part that gradually decreases upon heating. On the basis of these ^{13}C signals it is possible to quantify the partitioning of ester groups between the crystalline and amorphous phase as illustrated in Fig. 5c, using quantitative single-pulse ^{13}C MAS NMR. A deconvolution of both regions leads to ratios of 1 : 1.14 and 1 : 1.18 for the α-methoxy and methylene groups, respectively. Thus, the solid state NMR results demonstrate that the ester groups are uniformly distributed over the crystalline and amorphous phases in line with results from DSC and X-ray diffraction experiments.[60]

3.2 Bio-based polyamides

Polyamides belong to one of the most important groups of step-growth polymers due to their favorable and controllable physicochemical and mechanical properties.[72] For this reason they are extensively used in industry for injection molding, extrusion, and film or fiber applications. Recently, we have focused on bio-based polyamides created by incorporation of carbohydrate-derived 1,4:3,6-dianhydrohexitols (isohexides), since these are suitable building blocks for step-growth polymerization.[73–75]

Isohexides are secondary diols derived from C6-sugars, which can be obtained from starch or cellulose *via* a few (bio-)organic transformations.[76] Three isohexide isomers exist where the major conformer for each isomer is shown in Fig. 6a. These give rise to quite different ^{13}C chemical shifts (Fig. 6b) obtained from gas phase quantum chemical calculations (MP2/6-311G**).[75]

Variable-temperature solid state $^{13}C\{^{1}H\}$ CP/MAS NMR experiments were performed to determine the solid state behavior and stability of these isomers.[73–75] As reported by Gitsas *et al.*,[77] the dynamic changes of the local chain mobility of a polymer result in the reduction of the effective nuclear dipole–dipole couplings and thereby a lower CP efficiency at higher temperatures. Thus, by affecting the hydrogen bonding of the nano-structured polyamide chain fragments, the intensity of the signals originating from the crystalline phase will be affected more rapidly as a function of temperature compared with signals from the amorphous domains. As an example of the isohexide-based polyamides, Fig. 7a displays a series of VT solid state $^{13}C\{^{1}H\}$ CP/MAS NMR spectra for diamino-isosorbide (DAIS) when built into a regular polyamide structure

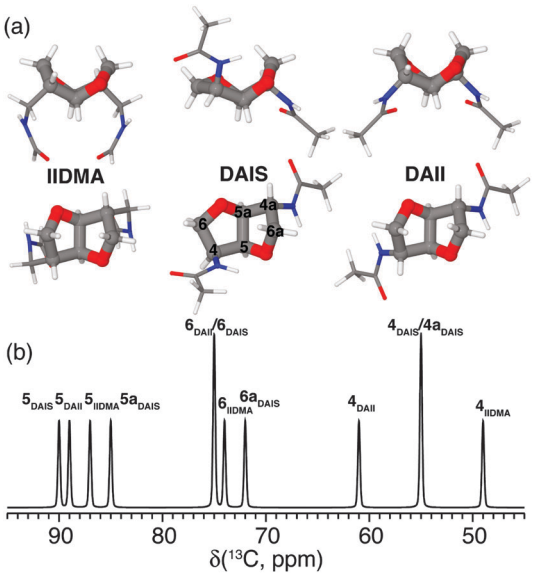

Fig. 6 (a) Top and side views of the most stable conformers for the primary diamines isoidide-2,5-dimethyleneamine (IIDMA, *endo–endo*), diaminoisosorbide (DAIS, *exo–endo*), and diaminoisoidide (DAII, *exo–exo*) found *via* gas phase MP2/6-311G** calculations. (b) Graphical representation of the calculated ^{13}C chemical shifts for all three conformers assigned using the nomenclature shown for DAIS in (a). Reprinted with permission from ref. 75. Copyright 2012, American Chemical Society.

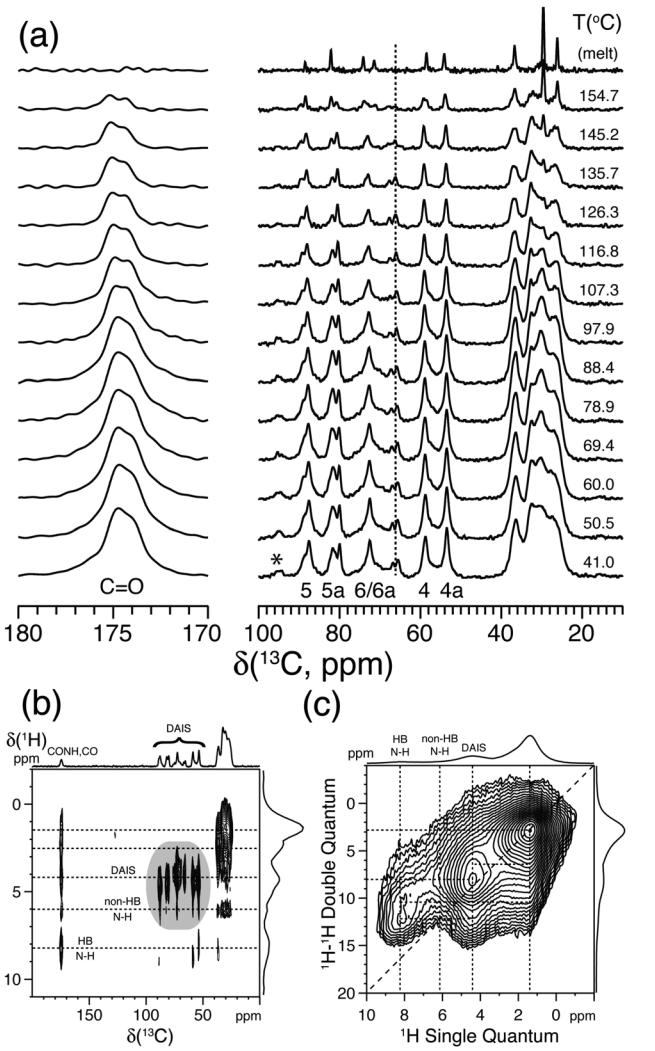

Fig. 7 (a) Variable-temperature solid state $^{13}C\{^{1}H\}$ CP/MAS NMR spectra of bio-based polyamide synthesized from sebacic acid and diamino-isosorbide (DAIS). (b) 2D $^{13}C\{^{1}H\}$ FSLG-HETCOR spectrum acquired using 2.0 ms CP. (c) 2D $^{1}H-^{1}H$ DQ-SQ spectrum recorded using a Back-to-Back (BaBa) recoupling/reconversion period of 67.2 μs. The dashed lines in (b) and (c) illustrate selected cross-peaks and autocorrelation peaks, including hydrogen-bonded (HB) and non-hydrogen-bonded (non-HB) amide fragments. Assignment is performed according to the scheme given in Fig. 6a. The asterisk indicates the position of a spinning sideband from the carbonyl resonance. Reprinted with permission from ref. 74, copyright 2012, American Chemical Society.

Open Access Article. Published on 18 2013. Downloaded on 14.03.2025 11:04:40.
This article is licensed under a Creative Commons Attribution 3.0 Unported Licence.

based on sebacic acid monomers. These spectra include well-resolved ^{13}C resonances originating from the C4 and C4a positions attached to the *exo* and *endo* oriented amide groups of DAIS. This suggests that the polymerization process does not affect the stereo configuration of the DAIS groups. Moreover, the resonances C5, C5a, and the amide C=O at 174.6 ppm exhibit lower intensities and shift to higher frequencies upon heating, while C5, C5a, C6, and C6a display significant changes in their intensities close to the melting point. The coexistence of these signals, albeit with different intensities close to the melting point, reflects the distribution of DAIS residues over the crystalline and amorphous domains of the sample. More significant intensity changes of the C5, C6, and C4 signals are observed above 100 °C, emphasizing the distribution of DAIS residues in both phases of the semi-crystalline polymer sample.

Further information about the molecular packing and hydrogen bonding of the DAIS-based polyamide can be derived from 2D $^{13}C\{^1H\}$ FSLG-HETCOR and ^1H–^1H DQ-SQ correlation experiments as shown in Fig. 7b and c. These spectra show that the DAIS-based polyamide includes two different types of amide groups which, based on the chemical shift difference and their position, are related to hydrogen-bonded (8.3 ppm) and non-hydrogen-bonded groups (6.0 ppm). The existence of two different hydrogen-bonding environments is also visible in Fig. 7a, where a doubling of the carbonyl resonance is observed. The two different hydrogen-bonding environments are most likely related to the non-crystalline and crystalline regions of the sample; however, no clear evidence for this behavior can be derived from the VT $^{13}C\{^1H\}$ CP/MAS NMR spectra in Fig. 7a, where both carbonyl signals show the same intensity decay as a function of temperature. Finally, the 2D ^1H–^1H DQ-SQ correlation spectrum reveals that the hydrogen-bonding environments are spatially separated (no cross-peak detected) and that the missing autocorrelation between the hydrogen-bonded amide groups points to a chain-folded structure, where these groups are not in close contact.

Thus, the above structural insights into the nano-structured ordering of isohexide-based polyamides from solid state NMR experiments combined with WAXD and DSC analysis show that the crystallinity, and hence the physical properties of the investigated compositions, can be tailored by the content of the bicyclic diamine in the backbone of the polyamides.[73–75]

3.3 Self-assembly and dynamics of polypeptides

Local chain conformations also play a vital role in the organization of polypeptides, *i.e.*, macromolecules composed of amino acids. Resembling biomacromolecules they have been considered for use in drug delivery and gene therapy and thus have been subject of intensive studies.[78,79] In addition, it is known that the superb performance of biological polypeptide-based materials such as hair or spiders' silk is due to a hierarchical superstructure over several length scales, where structure control is exerted at every level of hierarchy.[80]

The two most common local conformations of polypeptides, known as secondary structures, are the α-helix and the β-sheet, both stabilized by intramolecular hydrogen bonds. These secondary structures can be probed directly by solid state NMR[33] and their packing can be obtained by X-rays.[4] Over the years, we have studied

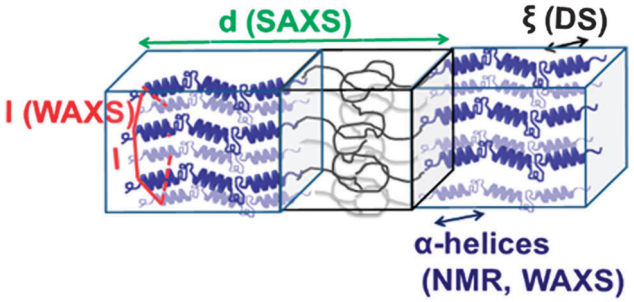

Fig. 8 Assembly of a lamellar forming polypeptide-coil diblock copolymer depicting the main techniques employed in our studies. Small-angle X-ray scattering (SAXS) is employed for the domain spacing, *d*. ^{13}C NMR and wide-angle X-ray scattering (WAXS) are employed to identify the type of the peptide secondary structure (α-helical in the schematic). WAXS is further employed to specify the lateral self-assembly of α-helices within the polypeptide domain (a hexagonal lattice is indicated in the schematic). Dielectric spectroscopy (DS) and site-specific NMR techniques are employed for the dynamics, taken from ref. 81.

various polypeptides by different NMR techniques, X-ray scattering, and dielectric spectroscopy in order to unravel their hierarchical self-assembly and dynamics as depicted in Fig. 8. The concerted application of these techniques shed light onto the origin of the glass transition, the persistence of the α-helical peptide secondary motif and the effects of topology and packing on the type and persistence of secondary structures.[81] Protein function and applications often depend on these issues. Using poly(γ-benzyl-L-glutamate), PBLG, as an example, it was shown that helices are objects of rather low persistence in the bulk as well as in concentrated solutions in helicogenic solvents.

Copolypeptides, on the other hand, with their inherent nanometer length scale of phase separation, provide means of manipulating both the type and persistence of peptide secondary structures. As examples we refer to the partial annihilation of α-helical structural defects due to chain stretching, to the induced chain folding of β-sheets in block copolypeptides with incommensurate dimensions, and to the destabilization of β-sheets in peptidic blocks having both secondary motifs.[77,82] These effects should be taken into account when such peptides are going to be employed *e.g.* in drug delivery.

Proline residues are of exceptional significance in protein conformation and protein folding as proline is the only amino acid where the nitrogen bears no amide hydrogen, preventing hydrogen bonding. Furthermore, the bulky pyrrolidine ring restricts the available conformations. Therefore, polypeptides with proline residues offer a unique possibility to unravel the interplay between hydrogen bonding and geometric packing effects. In a recent multitechnique study of diblock copolymers of PBLG and poly(L-proline) (PLP) their hierarchical self-assembly was investigated.[83] Both blocks possess helices stabilized either by hydrogen bonds (PBLG) or by steric hindrance (PLP) and are packed in two hexagonal cells of different dimensions. An intriguing *trans*/*cis* conformational change of PLP upon confinement was observed that mimics the isomerization of isolated proline residues in proteins. These *cis* PLP conformations reside primarily at the PLP/PBLG interface, alleviate the packing frustration as shown

Open Access Article. Published on 18 2013. Downloaded on 14.03.2025 11:04:40.
This article is licensed under a Creative Commons Attribution 3.0 Unported Licence.

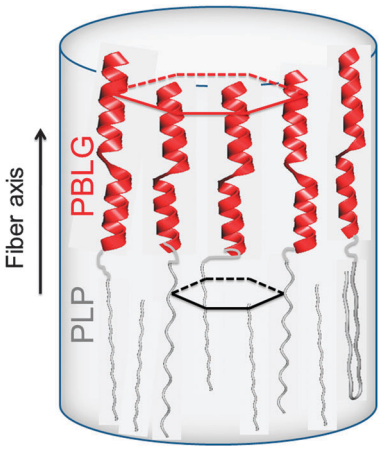

Fig. 9 Highly schematic representation of the copolymer self-assembly showing PBLG and PLP α-helices (NMR, WAXS) that are packed (WAXS) with significantly differently sized hexagons. The respective unit cells are indicated with red and black lines. The black arrow indicates the fiber axis, adopted from ref. 83.

in Fig. 9, and permit for PBLG and PLP helices to pack with the bulk.

Another important aspect of such systems that solid state NMR can tackle is the local chain dynamics, which might also be different for the two building blocks. Thermal analysis by differential scanning calorimetry (DSC), however, displayed a PBLG glass temperature in the copolymers without the indication of a second (PLP) glass temperature.[83] Information on the rigidity/dynamics of both polypeptides can be obtained from ^{13}C MAS NMR spectra recorded as a function of temperature.[77,81] Such spectra are depicted in Fig. 10 for PBLG-*b*-PLP

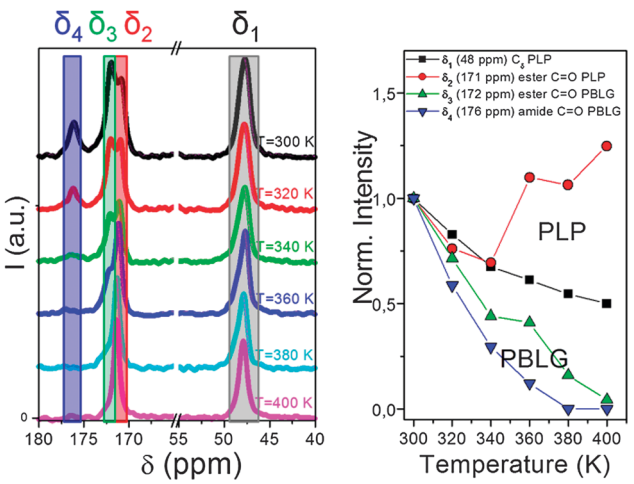

Fig. 10 (left) ^{13}C MAS NMR spectra of PBLG$_{73}$-*b*-PLP plotted as a function of temperature. Resonances at $\delta_1 \sim 48$ ppm, $\delta_2 \sim 171$ ppm, $\delta_3 \sim 172$ ppm and $\delta_4 \sim 176$ ppm correspond to the PLP C_δ, the PLP ester and to the PBLG side-group ester and amide carbons, respectively. (right) Temperature-dependence of the peak intensities corresponding to the above resonances. Notice the faster intensity drop for the PBLG resonances revealing a mobile PBLG backbone and a relatively rigid PLP backbone at the relevant parameters of the NMR experiment in the range of 20 kHz, adopted from ref. 83.

over the interesting spectral regions.[83] Evidently, the PLP C_δ and PBLG amide C=O resonances show distinctly different *T*-dependences. The former resonance loses about 40% of its integrated intensity in the *T*-range from 300 to 400 K, whereas the latter is reduced to a level that cannot be distinguished from the background noise. These intensity losses occur because the local peptide dynamics interfere with frequencies related to magic angle spinning, cross polarization, and dipolar decoupling all of the order of 20 kHz. Hence, the intensity corresponding to the $\delta_3 \sim 172$ ppm and the $\delta_4 \sim 176$ ppm resonances of PBLG is minimized at $\sim$400 K, suggesting that the underlying motional rates are about 20 kHz. This intensity drop for PBLG indicates low amplitude backbone motions of α-helical segments. However, within the same *T*-range, the PLP resonances are less affected. These results thus show a mobile PBLG backbone and a relatively rigid PLP backbone at the frequencies of the NMR experiment over the investigated *T*-range. This is consistent with the pronounced phase separation of the two polypeptides, where PBLG has a lower glass temperature and further indicates a much higher glass temperature for PLP.

4 Dynamic nuclear polarization involving macromolecules

Dynamic nuclear polarization (DNP) is a versatile technique used for NMR signal enhancement (commonly called hyperpolarization) thereby enabling new applications of this important method in natural sciences and medicine. As noted in the introduction, DNP relies on the transfer of the large equilibrium polarization from an electron spin ensemble to a nuclear spin ensemble and can thus be viewed as a 'marriage' of NMR and EPR. In soft matter, it usually requires the admixture of stable radicals to the sample and microwave irradiation at the frequency of the corresponding electron spin transitions. DNP can facilitate the NMR detection of nuclei with low natural abundance and/or low magnetogyric ratio, even in dilute solutions or for very small sample amounts.[84–86] Furthermore, it can dramatically reduce NMR measurement times, for example for multidimensional experiments on low natural abundance nuclei,[87] for the study of proteins,[17,88] or it can provide surface enhanced detection.[89] Last, but not least, DNP can be combined with ultrafast 2D spectroscopy.[90]

DNP experiments can be performed in the solid and in the liquid state. For the analysis of soft matter the combination of MAS NMR and solid state DNP is especially useful yet technically demanding.[91] However, during the last two decades a lot of progress has been made in this area culminating in the development of a commercially available solid state dynamic nuclear polarization-enhanced NMR spectrometer.[92] The milestones of this development were the implementation of high frequency microwave sources (gyrotrons[93]), low temperature MAS probes permitting *in situ* microwave irradiation of the samples[94] and biradical polarizing agents[95] drastically increasing the solid state DNP efficiency. However, DNP can also be applied in the liquid state for the investigation of dissolved macromolecules.

Open Access Article. Published on 18 2013. Downloaded on 14.03.2025 11:04:40.
This article is licensed under a Creative Commons Attribution 3.0 Unported Licence.

In the liquid phase, the transfer of polarization from electron to nuclear spins is governed by the Overhauser effect, which is mediated *via* cross relaxation mechanisms.[96]

In situ Overhauser DNP was realized decades ago at magnetic fields ranging from around 0.1 mT[97] up to 2.1 T.[98] Nowadays it can also be performed at magnetic fields up to 9.2 T[99] thus exploiting the excellent spectral resolution of modern high field NMR spectrometers. The DNP enhancement depends on the electron-nuclear coupling factor,[96] which in general reflects the dynamics and type of the molecular motions modulating the interaction between nuclear and electron spins. Its magnetic field dependence leads to slightly lower enhancements in Overhauser DNP at high magnetic fields.[100] High-field DNP also involves significant expense and technical effort, including gyrotron microwave sources and specialized cavity designs. Moreover, macromolecules exhibit considerably longer correlation times of molecular motion than solvents of low viscosity thereby further reducing the DNP coupling factor at higher magnetic fields.[96] Therefore, Overhauser DNP at moderate or low magnetic fields is obviously attractive, as for these magnetic fields affordable microwave sources, amplifiers and components are readily available and site selectivity can be provided by measuring different nuclei[101] or by using the spin-labeling techniques typical for EPR.

4.1 DNP enhancement of a hyperbranched polymer

As a recent example of this strategy we report on the ^{19}F-DNP enhancement of a biocompatible hyperbranched polymer[102] which has been used for molecular medical imaging employing ^{19}F MRI.[102] For these Overhauser DNP experiments we used an electromagnet (adjusted to 0.345 T) and an ENDOR probe, both manufactured by Bruker (Karlsruhe Germany). TEMPOL radicals (20 mM) were added to the ^{19}F containing hyperbranched polymers dissolved in water as a source of unpaired electron spins. Fig. 11 shows a ^{19}F DNP enhancement of −37, which equals an acquisition time saving of 1400 for ^{19}F NMR measurements. Indeed, as shown in Fig. 11 the DNP-enhanced spectrum (single shot) showed a slightly better signal-to-noise ratio than the reference spectrum acquired with 1000 scans.

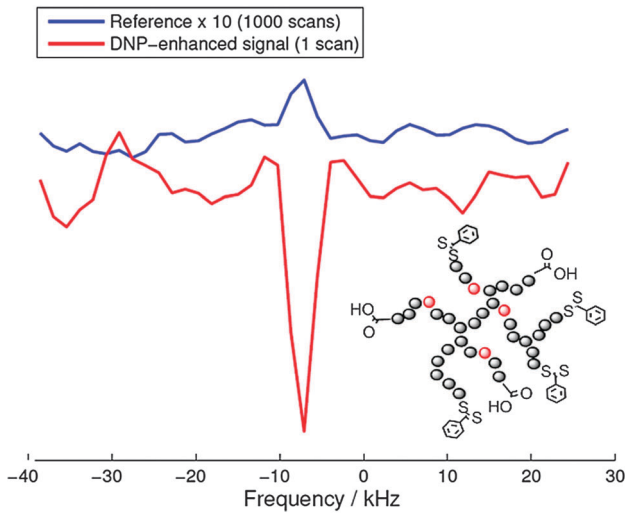

Fig. 11 Comparison of the reference spectrum (1000 scans) and the DNP-enhanced single-shot ^{19}F signal (1 scan) acquired on the same sample. The position of the ^{19}F containing and hyperpolarized moiety is indicated in red in the molecular structure of the hyperbranched polymer.

The fluorine atoms are located at the inner parts of the hyperbranched molecule which hinders the direct radical-^{19}F contact, which in turn significantly lowers the DNP coupling factor. This explains the reduced enhancement as compared to water protons (−110) under comparable conditions.[103] Nevertheless, this result opens up new possibilities for designing dual-mode MR imaging agents for medicine for measuring relatively fast biological processes with an additional imaging mechanism, where the DNP enhancement can overcome the less sensitive ^{19}F MRI.

4.2 Spin-labeled macromolecules as DNP polarizing agents

DNP with polymers offers a route to improved detection of such macromolecules.[104] Moreover, spin-labeling of macromolecules themselves can provide a new type of DNP polarizing agent. An interesting example of this strategy is the use of spin-labeled heparins[105,106] as biocompatible DNP polarizing agents. We have demonstrated how spin-labeling of macromolecules can lead to significantly higher DNP enhancements than free TEMPOL in the low-concentration regime.[107] This notably includes the absence of Heisenberg spin exchange and electron nuclear-spin relaxation (T_{1ne}), mixing the EPR hyperfine states due to collision of the radicals and relaxation of a coupled nuclear spin, respectively. Such behavior is of interest for the investigation of biomolecules at physiological temperatures where only small sample amounts can be provided and where high radical concentration leads to NMR-line broadening and fast nuclear T_1 relaxation. The chemical binding of the nitroxides to the heparin backbone is sketched in Fig. 12. It leads to a heterogeneous distribution and to an increased local concentration of electron spins as well as to reduced mobility. However, due to the stretched conformation of the heparin backbone the distance of closest approach between water molecules and spin-labels is almost unchanged as compared to free TEMPOL molecules. Therefore, the spin-labeled heparins exhibit almost the same coupling factor as free TEMPOL.[107] The electron spin-electron spin relaxation time T_{2e} on the other hand is decreased due to residual dipolar couplings and reduced mobility, resulting in broad EPR lines as shown in Fig. 12. Usually, for free radicals, broad EPR lines lead to low achievable DNP enhancement factors, because of incomplete saturation of the EPR lines. This, however, is not the case for the spin-labeled heparins where the achieved enhancement of $E = -110$ (see Fig. 12) proves directly that it is possible to effectively saturate more than one EPR hyperfine line. Moreover, the decreased electron spin–spin relaxation time could be identified as the reason for the high effective saturation even for small radical concentrations. Thus, despite being heterogeneously distributed, radicals attached to biomacromolecules can be used for DNP in cases where only small sample amounts are available.

 This journal is © the Owner Societies 2014

Open Access Article. Published on 18 2013. Downloaded on 14.03.2025 11:04:40.
This article is licensed under a Creative Commons Attribution 3.0 Unported Licence.

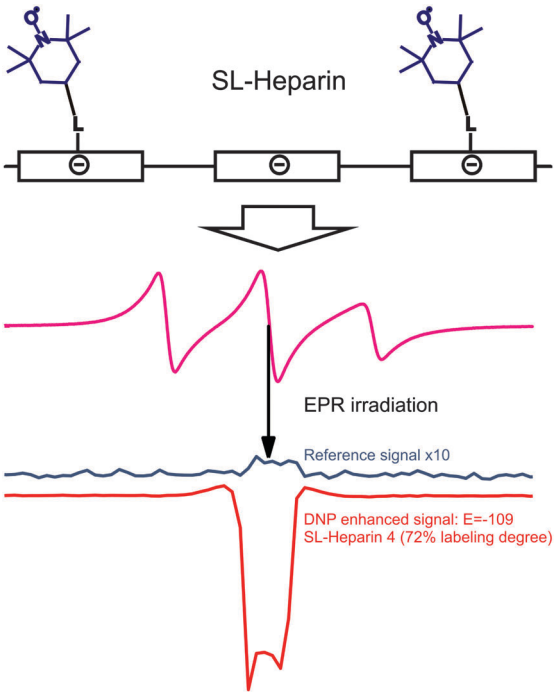

Fig. 12 Top row: schematic representation of the polyelectrolytic heparin with attached spin labels. Middle row: CW EPR spectrum of heparin with 72% of the monomer units labelled with TEMPOL dissolved in water. Bottom row: corresponding reference and DNP spectrum of the same sample.[108]

4.3 Thermoresponsive, spin-labeled, hydrophilic polymer networks as separable DNP polarizing agents

In NMR even small amounts of radicals can disturb the measurements because the radicals lead to increased NMR linewidths and/or decreased T_1. Therefore, methods for reliable, complete and fast radical removal after DNP hyperpolarization are sought. This would improve the applicability of DNP substantially and is particularly important for medical applications like metabolic imaging[109] of hyperpolarized substances because of the toxicity of certain radicals and the reduced lifetime of the accomplished hyperpolarization during the transport from the DNP polarizer to the MRI scanner. With these important aspects in mind we have introduced the application of thermoresponsive, spin-labeled hydrophilic polymer networks (SL-hydrogels) for DNP,[108] and demonstrated that they allow fast and simple radical–solute separation as depicted in Fig. 13. Heating the swollen hydrogel to a critical temperature T_C (63 °C) induces a reversible, fast ($\leq$1s) and dramatic volume decrease ($\geq$500 volume%) thereby expelling hyperpolarized water and other target molecules from the radical-bearing polymer network.

The SL-hydrogels used provided a maximum NMR signal enhancement for water of up to $E = -26.6 \pm 1.3$ (at 5 °C) at an incident microwave (mw) power of 2 W. For mw powers exceeding 2 W, we always observed a decline of the enhancement for all adjusted temperatures.[108] This indicates that the applied mw irradiation on the sample can induce a partial

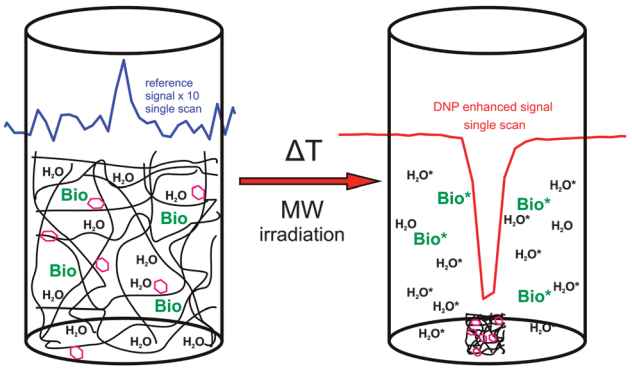

Fig. 13 Sketch of DNP polarization with a thermoresponsive spin-labeled hydrogel and subsequent temperature induced volume change resulting in the separation of the radicals and the hyperpolarized molecules (hexagon: spin-label, Bio: target biomolecules, *: hyperpolarized). The insets show the reference signal of the system at thermal equilibrium (blue) and the corresponding DNP-enhanced spectrum (red).

thermal collapse of the thermoresponsive SL-hydrogel due to local heating of the water even in a cooled system. The resulting spatial separation of the radicals, solvent and solute (resembling a micro-phase separation) leads to a diminished coupling factor before the sample is completely saturated, explaining the small DNP enhancement factors. The thermal collapse of our system limits the achievable DNP, but it provides the possibility of combining the saturation of the EPR lines and the separation of hyperpolarized target molecules and radicals in a single step. In addition, by the spatial separation after the thermal collapse, the spin–lattice relaxation time of the hyperpolarized molecules is prolonged up to T_1 values in the absence of radicals (T_1 = 2100 ms at 25 °C measured in water expelled from the hydrogel). For Overhauser DNP applications, the SL-hydrogels have to be further optimized to yield maximum DNP enhancement at room temperature. However, the specified features make SL-hydrogels very promising candidates for dissolution DNP[110] where the DNP polarization is accomplished at 1 K. The obvious benefits are the prolonged T_1 after the dissolution step, the radical-free and non-toxic solute containing the hyperpolarized biomolecules, allowing for biomedical applications. Furthermore, the severe heating effects, which occur at room temperature, should be overcome at lower temperatures, allowing for full saturation and maximum DNP enhancement of the sample.

5 Outlook and conclusions

This Perspective Article describes just a few examples of the application of advanced magnetic resonance spectroscopy to nanostructured soft matter. We feel that today's EPR spectroscopy combined with exploiting non-covalent self-assembly of spin probes bears great potential to reveal unusual properties of synthetic and disordered biological macromolecular systems.

Conformational studies of bio-based polymers and macromolecular systems by NMR will benefit strongly from the increased sensitivity offered by DNP and other hyperpolarizing methods. This will eventually allow studies of small sample volumes,

Open Access Article. Published on 18 2013. Downloaded on 14.03.2025 11:04:40.
This article is licensed under a Creative Commons Attribution 3.0 Unported Licence.

such as thin films. With ever increasing MAS spinning frequencies, merging of liquid- and solid state NMR techniques for studying structure and dynamics emerge.

Indeed, as pointed out recently by L. Emsley in an editorial[8] 'Recent advances in magnetic resonance allow the study of more and more complex molecular or materials problems, with a clear shift toward the study of systems *in situ* and toward real-time spectroscopy. Spectacular examples are appearing in the studies of human metabolism, the surface chemistry of catalysis or materials for energy, and the biological function of large assemblies. It is no coincidence that these are some of the most dynamics areas of chemistry today.' The examples provided in this Perspective Article should be taken as just a few examples along these lines.

Acknowledgements

Part of this work was supported by the Deutsche Forschungsgemeinschaft (DFG) under grant number HI 1094/2-1 and the Dutch Polymer Institute (DPI, project number 685). D.H. acknowledges support by the Max Planck Graduate Center with the University of Mainz (MPGC). M. R. H. acknowledges financial support from the Villum Foundation under the Young Investigator Programme. We thank D. L. Bryce for carefully checking the manuscript.

Notes and references

1 K. Matyjaszewski and M. Möller, *Polymer Science: A Comprehensive Reference*, Elsevier, 2012.
2 H. J. Dyson and P. E. Wright, *Nat. Rev. Mol. Cell Biol.*, 2005, **6**, 197–208.
3 J. M. Lehn, *Angew. Chem., Int. Ed. Engl.*, 1988, **27**, 89–112.
4 B. E. Warren, *X-ray Diffraction*, Dover Publications, 1969.
5 H. W. Spiess, *Macromolecules*, 2010, **43**, 5479–5491.
6 R. R. Ernst, G. Bodenhausen and A. Wokaun, *Principles of Nuclear Magnetic Resonance in One and Two Dimensions*, Clarendon Press, 1987.
7 K. Schmidt-Rohr and H. W. Spiess, *Multidimensional Solid-state NMR and Polymers*, Academic Press, 1994.
8 L. Emsley, *J. Am. Chem. Soc.*, 2013, **135**, 8089–8091.
9 A. Schweiger and G. Jeschke, *Principles of Pulse Electron Paramagnetic Resonance*, Oxford University Press, 2001.
10 G. Jeschke, *Annu. Rev. Phys. Chem.*, 2012, **63**, 419–446.
11 J. R. Yates, S. E. Dobbins, C. J. Pickard, F. Mauri, P. Y. Ghi and R. K. Harris, *Phys. Chem. Chem. Phys.*, 2005, **7**, 1402–1407.
12 G. Buntkowsky, H. Breitzke, A. Adamczyk, F. Roelofs, T. Emmler, E. Gedat, B. Grunberg, Y. P. Xu, H. H. Limbach, I. Shenderovich, A. Vyalikh and G. Findenegg, *Phys. Chem. Chem. Phys.*, 2007, **9**, 4843–4853.
13 M. C. D. Tayler and M. H. Levitt, *Phys. Chem. Chem. Phys.*, 2011, **13**, 5556–5560.
14 K. Möbius, A. Savitsky, A. Schnegg, M. Plato and M. Fuchs, *Phys. Chem. Chem. Phys.*, 2005, **7**, 19–42.
15 A. Abragam and W. G. Proctor, *C. R. Hebd. Seances Acad. Sci.*, 1958, **246**, 2253–2256.
16 G. T. Debelouchina, M. J. Bayro, P. C. A. van der Wel, M. A. Caporini, A. B. Barnes, M. Rosay, W. E. Maas and R. G. Griffin, *Phys. Chem. Chem. Phys.*, 2010, **12**, 5911–5919.
17 M. J. Bayro, G. T. Debelouchina, M. T. Eddy, N. R. Birkett, C. E. MacPhee, M. Rosay, W. E. Maas, C. M. Dobson and R. G. Griffin, *J. Am. Chem. Soc.*, 2011, **133**, 13967–13974.
18 K. Wuthrich, *Angew. Chem., Int. Ed.*, 2003, **42**, 3340–3363.
19 M. Hong and K. Schmidt-Rohr, *Acc. Chem. Res.*, 2013, **46**, 2154–2163.
20 S. P. Brown and H. W. Spiess, *Chem. Rev.*, 2001, **101**, 4125–4155.
21 A. Abragam, *The Principles of Nuclear Magnetism*, Clarendon Press, 1961.
22 A. Abragam and B. Bleaney, *Electron Paramagnetic Resonance of Transition Ions*, Oxford University Press, 1970.
23 P. Höfer, A. Grupp, H. Nebenfuhr and M. Mehring, *Chem. Phys. Lett.*, 1986, **132**, 279–282.
24 M. Pannier, S. Veit, A. Godt, G. Jeschke and H. W. Spiess, *J. Magn. Reson.*, 2000, **142**, 331–340.
25 W. L. Hubbell, D. S. Cafiso and C. Altenbach, *Nat. Struct. Biol.*, 2000, **7**, 735–739.
26 G. Jeschke and Y. Polyhach, *Phys. Chem. Chem. Phys.*, 2007, **9**, 1895–1910.
27 R. H. Acosta, P. Blümler, K. Munnemann and H. W. Spiess, *Prog. Nucl. Magn. Reson. Spectrosc.*, 2012, **66**, 40–69.
28 J. Schmidt, A. Hoffmann, H. W. Spiess and D. Sebastiani, *J. Phys. Chem. B*, 2006, **110**, 23204–23210.
29 S. P. Brown, *Solid State Nucl. Magn. Reson.*, 2012, **41**, 1–27.
30 D. Sebastiani, *ChemPhysChem*, 2006, **7**, 164–175.
31 A. E. Tonelli and F. C. Schilling, *Acc. Chem. Res.*, 1981, **14**, 233–238.
32 S. P. Brown, I. Schnell, J. D. Brand, K. Müllen and H. W. Spiess, *Phys. Chem. Chem. Phys.*, 2000, **2**, 1735–1745.
33 S. P. Brown, *Prog. Nucl. Magn. Reson. Spectrosc.*, 2007, **50**, 199–251. This article provides a comprehensive introduction to proton-proton correlation techniques in solid state NMR.
34 K. Müllen and J. P. Rabe, *Acc. Chem. Res.*, 2008, **41**, 511–520.
35 M. R. Hansen, R. Graf and H. W. Spiess, *Acc. Chem. Res.*, 2013, **46**, 1996–2007.
36 D. Demus, J. W. Goodby, G. W. Gray, H. W. Spiess and V. Vill, *Handbook of Liquid Crystals*, Wiley, 1998.
37 X. Feng, V. Marcon, W. Pisula, M. R. Hansen, J. Kirkpatrick, F. Grozema, D. Andrienko, K. Kremer and K. Muellen, *Nat. Mater.*, 2009, **8**, 421–426.
38 D. Adam, P. Schuhmacher, J. Simmerer, L. Haussling, K. Siemensmeyer, K. H. Etzbach, H. Ringsdorf and D. Haarer, *Nature*, 1994, **371**, 141–143.
39 M. R. Hansen, X. Feng, V. Macho, K. Müllen, H. W. Spiess and G. Floudas, *Phys. Rev. Lett.*, 2011, **107**, 257801.
40 L. J. Berliner, *Spin Labeling: Theory and Applications*, Academic Press, 1979.
41 S. A. Goldman, G. V. Bruno, C. F. Polnaszek and J. H. Freed, *J. Chem. Phys.*, 1972, **56**, 716–735.

Open Access Article. Published on 18 2013. Downloaded on 14.03.2025 11:04:40.
This article is licensed under a Creative Commons Attribution 3.0 Unported Licence.

42 O. A. Matthews, A. N. Shipway and J. F. Stoddart, *Prog. Polym. Sci.*, 1998, **23**, 1–56.
43 B. Z. Zhang, R. Wepf, K. Fischer, M. Schmidt, S. Besse, P. Lindner, B. T. King, R. Sigel, P. Schurtenberger, Y. Talmon, Y. Ding, M. Kroger, A. Halperin and A. D. Schluter, *Angew. Chem., Int. Ed.*, 2011, **50**, 737–740.
44 A. Sunder, R. Hanselmann, H. Frey and R. Mülhaupt, *Macromolecules*, 1999, **32**, 4240–4246.
45 M. J. N. Junk, W. Li, A. D. Schluter, G. Wegner, H. W. Spiess, A. Zhang and D. Hinderberger, *Macromol. Chem. Phys.*, 2011, **212**, 1229–1235.
46 D. Kurzbach, M. J. N. Junk and D. Hinderberger, *Macromol. Rapid Commun.*, 2013, **34**, 119–134.
47 M. J. N. Junk, H. W. Spiess and D. Hinderberger, *Angew. Chem., Int. Ed.*, 2010, **49**, 8755–8759.
48 Y. Akdogan, J. Reichenwallner and D. Hinderberger, *PLoS One*, 2012, **7**, e45681.
49 J. Reichenwallner and D. Hinderberger, *Biochim. Biophys. Acta, Gen. Subj.*, 2013, **1830**, 5382–5393.
50 D. Kurzbach, D. R. Kattnig, B. Z. Zhang, A. D. Schluter and D. Hinderberger, *J. Phys. Chem. Lett.*, 2011, **2**, 1583–1587.
51 D. Kurzbach, D. R. Kattnig, B. Z. Zhang, A. D. Schluter and D. Hinderberger, *Chem. Sci.*, 2012, **3**, 2550–2558.
52 D. Kurzbach, X. Q. Zhang, B. Z. Zhang, P. Arnold and D. Hinderberger, *Chem.–Eur. J.*, 2013, **19**, 5602–5608.
53 G. H. Bird, S. Pornsuwan, S. Saxena and C. E. Schafmeister, *ACS Nano*, 2008, **2**, 1857–1864.
54 D. Hinderberger, H. W. Spiess and G. Jeschke, *Appl. Magn. Reson.*, 2010, **37**, 657–683.
55 M. A. R. Meier, J. O. Metzger and U. S. Schubert, *Chem. Soc. Rev.*, 2007, **36**, 1788–1802.
56 F. Fenouillot, A. Rousseau, G. Colomines, R. Saint-Loup and J. P. Pascault, *Prog. Polym. Sci.*, 2010, **35**, 578–622.
57 P. Gallezot, *Chem. Soc. Rev.*, 2012, **41**, 1538–1558.
58 H. Mutlu, R. Hofsäß, R. E. Montenegro and M. A. R. Meier, *RSC Adv.*, 2013, **3**, 4927–4934.
59 N. Q. Ran, L. S. Zhao, Z. M. Chen and J. H. Tao, *Green Chem.*, 2008, **10**, 361–372.
60 M. P. F. Pepels, M. R. Hansen, H. Goossens and R. Duchateau, *Macromolecules*, 2013, **46**, 7668–7677.
61 H. M. Konig and A. F. M. Kilbinger, *Angew. Chem., Int. Ed.*, 2007, **46**, 8334–8340.
62 A. Bohle, G. Brunklaus, M. R. Hansen, T. W. Schleuss, A. F. M. Kilbinger, J. Seltmann and H. W. Spiess, *Macromolecules*, 2010, **43**, 4978–4985.
63 M. Wegner, D. Dudenko, D. Sebastiani, A. R. A. Palmans, T. F. A. de Greef, R. Graf and H. W. Spiess, *Chem. Sci.*, 2011, **2**, 2040–2049.
64 J. Shu, D. Dudenko, M. Esmaeili, J. H. Park, S. R. Puniredd, J. Y. Chang, D. W. Breiby, W. Pisula and M. R. Hansen, *J. Am. Chem. Soc.*, 2013, **135**, 11075–11086.
65 J. Lu, P. A. Mirau and A. E. Tonelli, *Prog. Polym. Sci.*, 2002, **27**, 357–401.
66 R. H. Grubbs, *Angew. Chem., Int. Ed.*, 2006, **45**, 3760–3765.
67 M. Kamigaito, T. Ando and M. Sawamoto, *Chem. Rev.*, 2001, **101**, 3689–3745.
68 S. Monsaert, A. L. Vila, R. Drozdzak, P. Van Der Voort and F. Verpoort, *Chem. Soc. Rev.*, 2009, **38**, 3360–3372.
69 T. W. Baughman and K. B. Wagener, in *Metathesis Polymerization*, ed. M. R. Buchmeiser, 2005, vol. 176, pp. 1–42.
70 Y. Y. Wei, R. Graf, J. C. Sworen, C. Y. Cheng, C. R. Bowers, K. B. Wagener and H. W. Spiess, *Angew. Chem., Int. Ed.*, 2009, **48**, 4617–4620.
71 R. G. Alamo, K. Jeon, R. L. Smith, E. Boz, K. B. Wagener and M. R. Bockstaller, *Macromolecules*, 2008, **41**, 7141–7151.
72 C. J. Luo, S. D. Stoyanov, E. Stride, E. Pelan and M. Edirisinghe, *Chem. Soc. Rev.*, 2012, **41**, 4708–4735.
73 L. Jasinska-Walc, M. Villani, D. Dudenko, O. van Asselen, E. Klop, S. Rastogi, M. R. Hansen and C. E. Koning, *Macromolecules*, 2012, **45**, 2796–2808.
74 L. Jasinska-Walc, D. Dudenko, A. Rozanski, S. Thiyagarajan, P. Sowinski, D. van Es, J. Shu, M. R. Hansen and C. E. Koning, *Macromolecules*, 2012, **45**, 5653–5666.
75 J. Wu, L. Jasinska-Walc, D. Dudenko, A. Rozanski, M. R. Hansen, D. van Es and C. E. Koning, *Macromolecules*, 2012, **45**, 9333–9346.
76 G. Flèche and M. Huchette, *Starch/Stärke*, 1986, **38**, 26–30.
77 A. Gitsas, G. Floudas, M. Mondeshki, I. Lieberwirth, H. W. Spiess, H. Iatrou, N. Hadjichristidis and A. Hirao, *Macromolecules*, 2010, **43**, 1874–1881.
78 H. A. Klok and S. Lecommandoux, in *Peptide Hybrid Polymers*, ed. H. A. Klok and H. Schlaad, Springer-Verlag Berlin, Berlin, 2006, vol. 202, pp. 75–111.
79 J. R. McDaniel, D. J. Callahan and A. Chilkoti, *Adv. Drug Delivery Rev.*, 2010, **62**, 1456–1467.
80 R. Tycko, *Annu. Rev. Phys. Chem.*, 2001, **52**, 575–606.
81 G. Floudas and H. W. Spiess, *Macromol. Rapid Commun.*, 2009, **30**, 278–298.
82 T. Aliferis, H. Iatrou and N. Hadjichristidis, *Biomacromolecules*, 2004, **5**, 1653–1656.
83 R. Graf, H. W. Spiess, G. Floudas, H. J. Butt, M. Gkikas and H. Iatrou, *Macromolecules*, 2012, **45**, 9326–9332.
84 F. Blanc, L. Sperrin, D. A. Jefferson, S. Pawsey, M. Rosay and C. P. Grey, *J. Am. Chem. Soc.*, 2013, **135**, 2975–2978.
85 O. Ouari, T. Phan, F. Ziarelli, G. Casano, F. Aussenac, P. Thureau, D. Gigmes, P. Tordo and S. Viel, *ACS Macro Lett.*, 2013, **2**, 715–719.
86 R. G. Griffin and T. F. Prisner, *Phys. Chem. Chem. Phys.*, 2010, **12**, 5737–5740.
87 H. Takahashi, D. Lee, L. Dubois, M. Bardet, S. Hediger and G. De Paepe, *Angew. Chem., Int. Ed.*, 2012, **51**, 11766–11769.
88 E. Ravera, B. Corzilius, V. K. Michaelis, C. Rosa, R. G. Griffin, C. Luchinat and I. Bertini, *J. Am. Chem. Soc.*, 2013, **135**, 1641–1644.
89 A. Lesage, M. Lelli, D. Gajan, M. A. Caporini, V. Vitzthum, P. Mieville, J. Alauzun, A. Roussey, C. Thieuleux, A. Mehdi, G. Bodenhausen, C. Coperet and L. Emsley, *J. Am. Chem. Soc.*, 2010, **132**, 15459–15461.
90 L. Frydman and D. Blazina, *Nat. Phys.*, 2007, **3**, 415–419.

Open Access Article. Published on 18 2013. Downloaded on 14.03.2025 11:04:40.
This article is licensed under a Creative Commons Attribution 3.0 Unported Licence.

91 Q. Z. Ni, E. Daviso, T. V. Can, E. Markhasin, S. K. Jawla, T. M. Swager, R. J. Temkin, J. Herzfeld and R. G. Griffin, *Acc. Chem. Res.*, 2013, **46**, 1933–1941.
92 http://www.bruker.com/products/mr/nmr/dnp-nmr/overview.html.
93 V. S. Bajaj, M. K. Hornstein, K. E. Kreischer, J. R. Sirigiri, P. P. Woskov, M. L. Mak-Jurkauskas, J. Herzfeld, R. J. Temkin and R. G. Griffin, *J. Magn. Reson.*, 2007, **189**, 251–279.
94 A. B. Barnes, E. A. Nanni, J. Herzfeld, R. G. Griffin and R. J. Temkin, *J. Magn. Reson.*, 2012, **221**, 147–153.
95 C. Song, K.-N. Hu, C.-G. Joo, T. M. Swager and R. G. Griffin, *J. Am. Chem. Soc.*, 2006, **128**, 11385–11390.
96 K. H. Hausser and D. Stehlik, *Adv. Magn. Reson.*, 1968, **3**, 79–139.
97 E. H. Poindexter, J. A. Potenza, D. D. Thompson, N. Vannghia and R. H. Webb, *Mol. Phys.*, 1968, **14**, 385–391.
98 H. Brunner and K. H. Hausser, *J. Magn. Reson.*, 1972, **6**, 605–611.
99 V. P. Denysenkov, M. J. Prandolini, A. Krahn, M. Gafurov, B. Endeward and T. F. Prisner, *Appl. Magn. Reson.*, 2008, **34**, 289–299.
100 N. M. Loening, M. Rosay, V. Weis and R. G. Griffin, *J. Am. Chem. Soc.*, 2002, **124**, 8808–8809.
101 O. Neudert, C. Mattea, H. W. Spiess, S. Stapf and K. Muennemann, *Phys. Chem. Chem. Phys.*, 2013, **15**, 20717–20726.
102 K. J. Thurecht, I. Blakey, H. Peng, O. Squires, S. Hsu, C. Alexander and A. K. Whittaker, *J. Am. Chem. Soc.*, 2010, **132**, 5336–5337.
103 M.-T. Turke and M. Bennati, *Phys. Chem. Chem. Phys.*, 2011, **13**, 3630–3633.
104 V. Vitzthum, F. Borcard, S. Jannin, M. Morin, P. Mieville, M. A. Caporini, A. Sienkiewicz, S. Gerber-Lemaire and G. Bodenhausen, *ChemPhysChem*, 2011, **12**, 2929–2932.
105 A. L. Kleschyov, V. Sen, V. Golubev, K. Munnemann, D. Hinderberger, K. J. Lackner, S. Weber, M. Terekhov, L. M. Schreiber and T. Munzel, *Eur. J. Med. Chem.*, 2012, **58**, 265–271.
106 R. Lever, B. Mulloy and C. P. Page, *Heparin - A Century of Progress*, Springer, 2012.
107 B. C. Dollmann, A. L. Kleschyov, V. Sen, V. Golubev, L. M. Schreiber, H. W. Spiess, K. Munnemann and D. Hinderberger, *ChemPhysChem*, 2010, **11**, 3656–3663.
108 B. C. Dollmann, M. J. N. Junk, M. Drechsler, H. W. Spiess, D. Hinderberger and K. Munnemann, *Phys. Chem. Chem. Phys.*, 2010, **12**, 5879–5882.
109 K. Golman, R. Zandt, M. Lerche, R. Pehrson and J. H. Ardenkjaer-Larsen, *Cancer Res.*, 2006, **66**, 10855–10860.
110 J. H. Ardenkjaer-Larsen, B. Fridlund, A. Gram, G. Hansson, L. Hansson, M. H. Lerche, R. Servin, M. Thaning and K. Golman, *Proc. Natl. Acad. Sci. U. S. A.*, 2003, **100**, 10158–10163.

This journal is © the Owner Societies 2014